Journal of Power Sources 229 (2013) 72–78

Contents lists available at SciVerse ScienceDirect

Journal of Power Sources

journal homepage: www.elsevier.com/locate/jpowsour

In situ intercalative polymerization of pyrrole in graphene analogue of MoS_2 as advanced electrode material in supercapacitor

Guofu Ma*, Hui Peng, Jingjing Mu, Haohao Huang, Xiaozhong Zhou, Ziqiang Lei*

Key Laboratory of Eco-Environment-Related Polymer Materials of Ministry of Education, Key Laboratory of Polymer Materials of Gansu Province, College of Chemistry and Chemical Engineering, Northwest Normal University, Lanzhou 730070, China

HIGHLIGHTS

- Flowerlike MoS_2 with graphene-like structure is prepared by hydrothermal method.
- The PPy/MoS_2 nanocomposite is prepared by in situ oxidation polymerization.
- The MoS_2 provides a path for insertion and extraction of ions within PPy.
- This PPy/MoS_2 nanocomposite exhibit high capacity and excellent cycling stability.

GRAPHICAL ABSTRACT

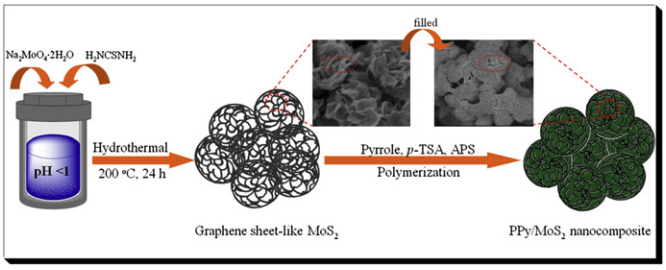

ARTICLE INFO

Article history:
Received 20 June 2012
Received in revised form
13 October 2012
Accepted 24 November 2012
Available online 2 December 2012

Keywords:
Molybdenum disulfide
Polypyrrole
Nanocomposite
Supercapacitor

ABSTRACT

We report a facile strategy to synthesize of polypyrrole/molybdenum disulfide (PPy/MoS_2) nanocomposite as an advanced electrode material for high-performance supercapacitors applications. Flowerlike MoS_2 with graphene-like subunits structure is prepared using a hydrothermal method, and the nanocomposite PPy are embedded in MoS_2 nanosheets is prepared by in situ oxidation polymerization of pyrrole in the presence of MoS_2 suspension. Structural and morphological characterizations of the nanocomposite are investigated by XRD, FE-SEM and TEM measurements. Their electrochemical properties are also investigated using cyclic voltammetry, and galvanostatic charge/discharge. The PPy/MoS_2 nanocomposite exhibit high specific capacitance of 553.7 F g^{-1} and its capacitance can still remain 90% after 500 cycles at a current density of 1 A g^{-1}.

1. Introduction

Supercapacitor also called electrochemical capacitor has become one of the most promising energy storage devices due to it can deliver high levels of electrical power and offer long operating lifetimes [1–3]. Supercapacitors may be divided into two mechanisms that occur at or near the electrode/electrolyte interfaces in the capacitors [4]. The first is double-layer capacitance, which is a non-Faradic process such as carbon materials as electrode materials [5], and the other is redox capacitive mechanisms pseudo-capacitance, which is a Faradic process such as some metal oxides and conducting polymers as electrode materials [6,7]. To improve the electric conductivity and specific capacitance of the active electrode materials used in the supercapacitors, these two mechanisms usually work together.

Recently, graphene materials have been extensively studied and applied in optoelectronic, electronic, capacitor applications, due to its high electrical conductivity, large surface area, unique

* Corresponding authors. Tel./fax: +86 931 7970359.
E-mail addresses: magf@nwnu.edu.cn (G. Ma), hhhuang@nwnu.edu.cn (H. Huang), leizq@nwnu.edu.cn, leizq1958@hotmail.com (Z. Lei).

0378-7753/$ – see front matter © 2012 Elsevier B.V. All rights reserved.
http://dx.doi.org/10.1016/j.jpowsour.2012.11.088

heterogeneous electron transfer and great chemical stability [2,8,9]. Nevertheless, this material is generally expensive, low yield, and poor scalability [10,11]. But metal sulfides MoS_2 which are analogues of graphene (have a graphene-like single-layer structure) [12] can be easy synthesized. It is composed of three atom layers (S–Mo–S) stacked together through van der Waals interactions [13] and can be exfoliated to a single-layer or few-layer structure by chemical or physical methods [12,14,15]. It has attracted great interest in lithium ion batteries, catalysis, phototransistors due to their unique morphology, excellent mechanical and electrical properties [16–19]. In addition, Soon and Lohz [20] reported that the MoS_2 also used as an electrode material for capacitor due to their sheet-like morphology, which provides large surface area for double-layer charge storage. And it is found that the supercapacitor performance of MoS_2 is comparable to that of carbon nanotube array electrodes. However, attractive carbon nanotubes are still very expensive and their preparation process is relatively complex. In addition to double-layer capacitance, diffusion of the ions into the MoS_2 at slow scan rates gives rise to faradaic capacitance, which play an important role in enhancing charge storage capabilities, but, the specific capacitance of MoS_2 is still very limited in alone for energy storage applications.

Among the electrode material, the conducting polymer based supercapacitor has attracted much attention because of its high energy density, low cost, easy synthesis, and environmental friendliness [21,22]. Among the conducting polymers for the supercapacitor, such as polypyrrole (PPy), polyaniline (PANI), poly (3-methylthiopin), PPy is an intrinsically conducting polymer because of its high conductivity, high storage ability, good thermal and environmental stability, high redox and capacitive current and biocompatibility [23]. However, it has a relatively poor cycling stability and temperature dependence [24], because the redox sites in the polymer backbone are not sufficiently stable and the backbone of polymer can be destroyed within a limited number of charge/discharge cycles. Therefore, it is often hybridized with inorganic materials (carbon materials, metal oxides) or organic materials to prepare a composite and used in supercapacitors with better cycleability, specific capacitance and mechanical stability [23,25–27]. An et al. [23] prepared the Polypyrrole/carbon aerogel composite materials by chemical oxidation polymerization through ultrasound irradiation for supercapacitors, which composite material has a high specific capacitance of 433 F g^{-1} and excellent cycling stability. Sharma and co-workers [26] electrochemical synthesis of the MnO_2 embedded PPy nanocomposite as an electrode material for supercapacitor, which specific capacitance of the nanocomposite is remarkably high (620 F g^{-1}) in comparision to its constituents MnO_2 and PPy, and it shows long redox cycling life. We have found that polyaniline/sodium carboxymethyl cellulose hybrid material has an excellent specific capacitance and good rate capability at large current densities [27]. However, the conductive polymer and metal sulfide composite materials for supercapacitors are rarely reported.

Herein, we report a facile strategy to synthesize the nanocomposite PPy are embedded in MoS_2 nanosheets by in situ oxidation polymerization of pyrrole in the presence of MoS_2 suspension. MoS_2 as a polymerization substrates in the polymerization system and provides a path for the insertion and extraction of ions within the PPy, and ensures a high reaction rate. Electrochemical tests indicate that the PPy/MoS_2 nanocomposite exhibit very high capacity and excellent cycling stability as electrode materials for supercapacitors. In addition, this synthesis method presents a promising general route for the large-scale production of PPy/MoS_2 composites as energy storage materials.

2. Experimental

2.1. Materials

Pyrrole monomer (Shanghai Chemical Works, China) was distilled under reduced pressure. Ammonium persulfate ($(NH_4)_2S_2O_8$, APS, Tianjing Damao Chemical Co., China), sodium molybdate ($Na_2MoO_4 \cdot 2H_2O$, Tianjing Chemical Co., China), thiourea (H_2NCSNH_2, Shandong Shuangshuang Chemical Co., China), *P*-toluenesulfonic acid ($C_7H_8O_3S \cdot H_2O$, *P*-TSA, Shanghai Chemical Works, China), Solutions were prepared using deionized water. All other chemical reagents were in analytical grade.

2.2. Synthesis of molybdenum disulfide

The flowerlike MoS_2 with graphene-like subunits structure was synthesized as follows: 2.19 g of $Na_2MoO_4 \cdot 2H_2O$ (9 mmol) and 2.07 g of H_2NCSNH_2 (27 mmol) were dissolved in 70 ml deionized water under violent stirring. After stirring for 10 min approximately, 12 M HCl was added into the above solution mixture drop by drop under stirring to adjust the pH value to less than 1. Finally, the solution was transferred into a 100 ml Teflon-lined stainless steel autoclave and heated at 200 °C for 24 h. After cooled to room temperature naturally, the resulting black precipitates of MoS_2 were collected by filtration, washed with distilled water and absolute ethanol for several times to remove the residue of reactants, and then dried in vacuum at 60 °C for 24 h.

2.3. Synthesis of PPy/MoS_2 nanocomposite

Polypyrrole/molybdenum disulfide composites were synthesized by in situ chemical oxidative polymerization directed by molybdenum disulfide. In a typical process, 0.25 g molybdenum disulfide and 1.14 g *P*-toluenesulfonic acid was ultrasonic dispersed in 30 ml deionized water at ambient temperature. Then, the solution was transferred into ice bath, cooled to below 5 °C, 0.5 g pyrrole monomer was dispersed in above solution under violent stirring. After stirring for 30 min, 0.82 g $(NH_4)_2S_2O_8$ (dissolved in 10 ml deionized water) was dropped into above solution. The polymerization was performed for at least 12 h at ice bath. Reaction product was collected by centrifugation and washed successively with deionized water and ethanol and then dried at 60 °C for 24 h under vacuum to obtain a black powder.

For comparison purpose, pure polypyrrole without molybdenum disulfide was synthesized under same conditions.

2.4. Characterizations

X-ray diffraction (XRD) of samples was performed on a diffractometer (D/Max-2400, Rigaku) advance instrument using Cu Kα radiation ($k = 1.5418$ Å) at 40 kV, 100 mA. The 2θ range used in the measurements was from 5 to 80°. The surface morphology of the MoS_2, pure PPy and PPy/MoS_2 composites were examined with field emission scanning electron microscopy (FE-SEM, JSM-6701F Japan) at an accelerating voltage of 5.0 kV. The structure of the samples was characterized by a transmission electron microscopy (TEM, JEM-2010 Japan). The zeta potentials of MoS_2 aqueous dispersions were measured by the use of a zetasizer nanosystem (Nano ZS, Malvern Instruments).

2.5. Electrochemical measurements

A typical three-electrode test cells in electrolyte was used for electrochemical measurement on CHI650D (Chenghua, Shanghai China) electrochemical working station. All the measurements

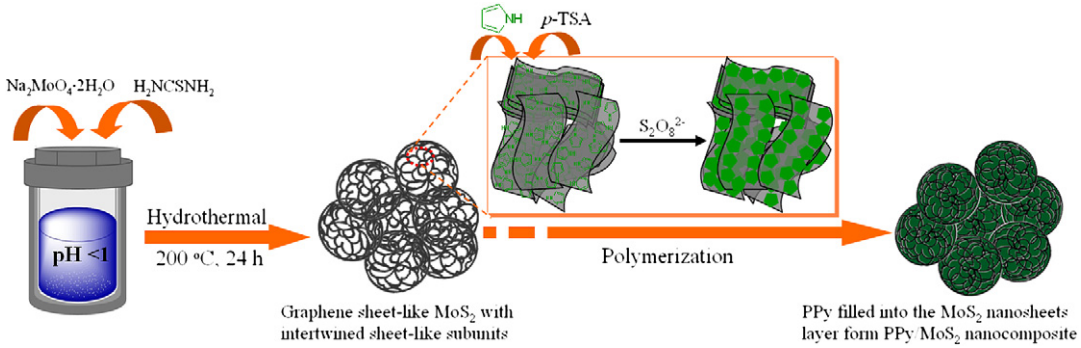

Scheme 1. Schematic of the preparation process of PPy/MoS_2 nanocomposite.

were carried out in 1 M KCl electrolyte at room temperature. The glassy carbon electrode with a diameter of 3 mm was used as the working electrode. Platinum electrode served as the counter electrode and saturated calomel electrode (SCE) as the reference electrode. The working electrodes were fabricated similar to our previous reported literature [27]. Typically, 4 mg of PPy/MoS_2 was ultrasonically dispersed in 1 ml of deionized water, and 10 μl of the polytetrafluoroethylene (PTFE) preparation emulsion (60 wt%) was added to the dispersion. The above suspension of 3 μl using a pipet gun was dropped onto the glassy carbon electrode and dried at room temperature.

Cyclic voltammograms were recorded from −0.8 to 0.5 V at scan rates of 10, 25, 50, 75 and 100 mV s^{-1}. The galvanostatic charge/discharge property and measurement of cycle-life stability were performed using computer controlled cycling equipment (LAND CT2001A, Wuhan China). The galvanostatic charge/discharge property was measured at the current densities of 1, 2, 3, 5, and 10 A g^{-1} with cutoff voltage of −0.5 to 0.3 V.

3. Results and discussion

3.1. Mechanism of the formation of the PPy/MoS_2 nanocomposite

The synthesis of polypyrrole/molybdenum disulfide nanocomposite was conducted through in situ oxidation polymerization of pyrrole in the presence of molybdenum disulfide suspension, as described in Scheme 1. On the basis of the common knowledge concerning elemental sulfur and its compounds, the possible reaction routes for the synthesis of MoS_2 by sodium molybdate and thiourea could be formulated as:

$$NH_2CSNH_2 + 2H_2O = 2NH_3\uparrow + H_2S + CO_2\uparrow \quad (1)$$

$$4Na_2MoO_4 + 9H_2S + 6HCl = 4MoS_2 + Na_2SO_4 + 12H_2O + 6NaCl \quad (2)$$

As shown in Fig. 1, the MoS_2 nanosheets is negatively charged (zeta potential = −36 mV) in neutral aqueous solution, which is similar to the graphite oxide (zeta potential approximately −40 mV in neutral aqueous solution) [28]. The *P*-toluenesulfonic acid serves as a dopant for polypyrrole, when pyrrole monomer was added into the MoS_2 suspension, due to electrostatic interaction between negatively charged of MoS_2 nanosheets and positive charge of pyrrole monomer, as a result, the pyrrole monomer was adsorbed on the surface of MoS_2 nanosheets.

After the oxidant ammonium persulfate was added into the system, polypyrrole was synthesized and it was attached onto the surface of MoS_2 nanosheets. As a result, the polypyrrole/molybdenum disulfide nanocomposite was prepared.

3.2. The morphology and structure of PPy/MoS_2 nanocomposite

The X-ray powder diffraction patterns of the MoS_2, pure PPy and PPy/MoS_2 nanocomposite powders are shown in Fig. 2. It can be seen that diffraction of pure PPy shows a typical broad and weak reflection located in the range of 15–30°, which are the characteristic peak of amorphous PPy. The pure MoS_2 has the diffraction peaks at 2θ = 14, 33, 44 and 59° can be unambiguously assign to the (002), (100), (103), and (110) planes of MoS_2 (JCPDS No.37-1492), respectively [29]. For the PPy/MoS_2 nanocomposite, it has a similar X-ray diffraction patterns to MoS_2. However, the peak of PPy/MoS_2 nanocomposite exhibits another broad reflection located in the range of 20–30°, which is different from the peak of MoS_2. This is attributed to the diffraction patterns of PPy, and the results also confirm that the PPy was successfully attached into the MoS_2 nanosheets layer.

FE-SEM technique was employed to vividly depict the morphology of the MoS_2, pure PPy and PPy/MoS_2 nanocomposite powders are shown in Fig. 3. It is very obvious that the MoS_2 (Fig. 3a) is flowerlike with intertwined sheet-like subunits structure, and the diameter of the flowerlike structure approximately 300 nm. One can see that pure PPy particles (Fig. 3b) aggregate into agglutinate small spheres. They do not have regular morphology because pyrrole polymerization is a multi-level growth process. But in situ oxidation polymerization of pyrrole in the presence of MoS_2 suspension, PPy could fill into the MoS_2 nanosheets layer. As shown in Fig. 3c, we can clearly see that the PPy are embedded in MoS_2 nanosheets form PPy/MoS_2 nanocomposite, and some MoS_2 is packaged by PPy, However, the MoS_2 nanosheets edges still clearly visible.

This interesting structure of MoS_2 and PPy/MoS_2 nanocomposite were further characterized by transmission electron microscopy (TEM). It is very obvious that the product of MoS_2 (Fig. 4a) shows thin layers folded and tangled together morphology. As shown in Fig. 4b, the MoS_2 nanosheets are embedded in PPy, with some possessing folded edges exhibiting parallel lines corresponding to the different layers of MoS_2 sheets (layer number ~ 4–10, Fig. 4c).

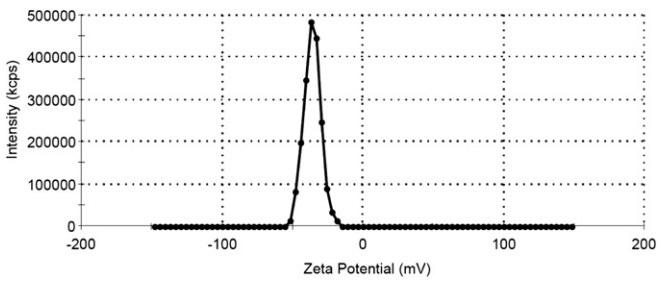

Fig. 1. Zeta potential curve of the MoS_2 nanosheets suspension in neutral aqueous solution.

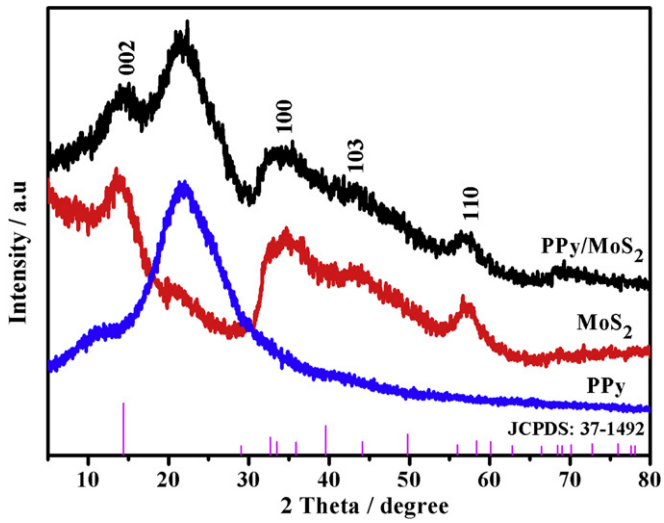

Fig. 2. XRD patterns of MoS_2, pure PPy and PPy/MoS_2 nanocomposites.

3.3. Electrochemical characteristics of PPy/MoS_2 nanocomposite electrode

In order to evaluate the electrochemical properties of the MoS_2, pure PPy and PPy/MoS_2 nanocomposite, cyclic voltammetry (CV) and galvanostatic charge/discharge tests were performed. The CV curves for the MoS_2, pure PPy and PPy/MoS_2 nanocomposite electrodes are presented in Fig. 5 at a scanning rate of 50 mV s^{-1} in the potential window of −0.8 to 0.5 V versus SCE in 1 M KCl. The CV curve of the MoS_2 show a rectangular shape without any obvious redox peaks, which indicates that MoS_2 at fast scan rates possesses a typical electrical double-layer capacitance, the result similar to the previous reported literature [20]. However, the capacitance characteristic of pure PPy or PPy/MoS_2 nanocomposite is distinct from that of the electric double-layer capacitance and the curves close to the ideal rectangular shape with pseudocapacitance characteristics. We can see that both pure PPy and PPy/MoS_2 nanocomposite curves posses a couple of redox peak, indicating the insertion and expulsion of K^+ ions [30]. And the shape does not have remarkable change except for the output current of PPy/MoS_2 nanocomposite is higher than that of pure PPy. Since the current for the same active weight represents the capacitance at the same sweep rate, obviously, PPy/MoS_2 nanocomposite electrode possessed a high capacitance than pure PPy and MoS_2 electrode. This result could be attributed to the intimate interaction between the PPy and MoS_2 substrates layers through in situ oxidation polymerization method, which was facilitated to MoS_2 electrochemically active since charge carriers could be effectively and rapidly conducted back and forth from MoS_2 nanosheets layers edges to inside and outside of PPy [17,20]. Therefore, the excellent electrochemical properties of the PPy/MoS_2 nanocomposite are attributed to the integral composite structure and the synergistic effect between PPy and MoS_2 substrates.

In order to further research the properties of the PPy/MoS_2 nanocomposite electrode, Fig. 6 shows the CV curves of the composite electrode at various scan rates. CV curve area increases with increasing scan rate, with the increase of a scan rate from 5 to 100 mV s^{-1}, the peak current rapidly increased from 0.05 to 1.12 mA, the redox peaks are observed in the curve even at scan rates 100 mV s^{-1}. Consequently, the PPy/MoS_2 nanocomposite electrode has a good rate ability of in 1 M KCl solution. And the CVs are nearly rectangular, indicating fast charging/discharging processes.

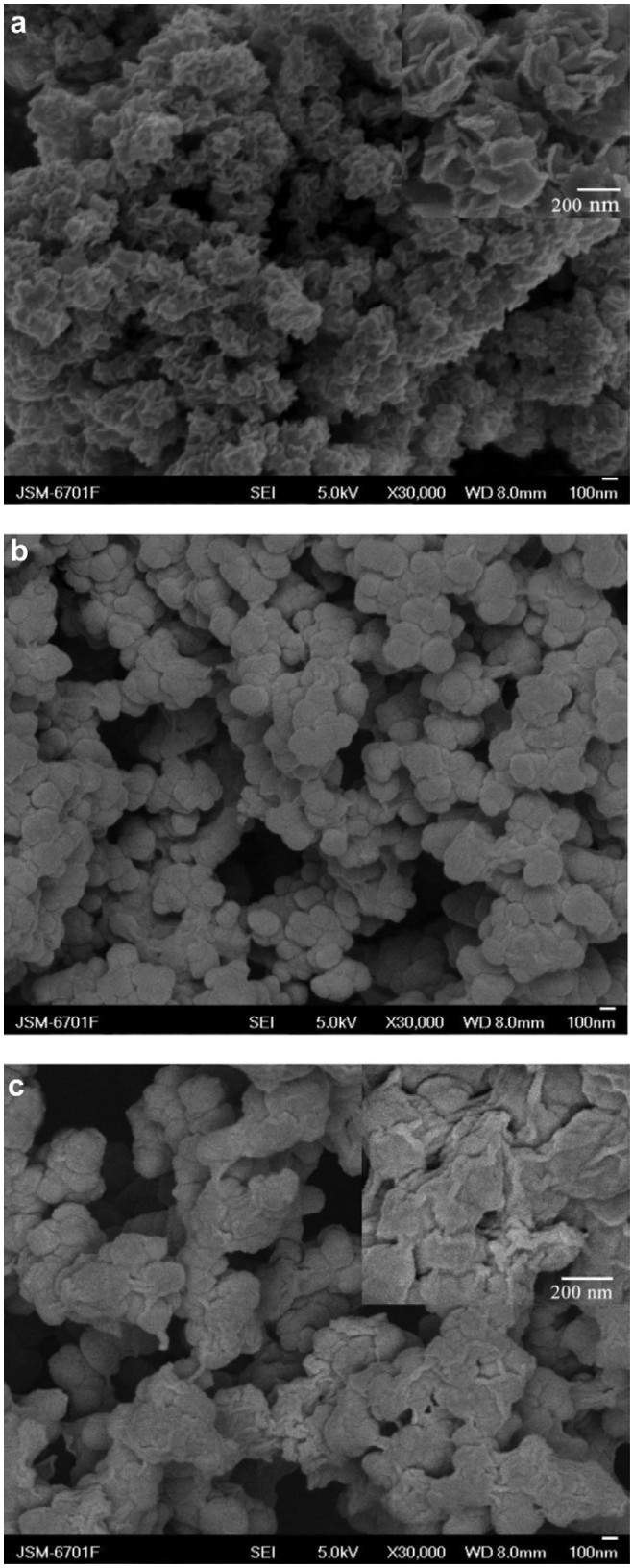

Fig. 3. SEM images of (a) MoS_2 (b) pure PPy and (c) PPy/MoS_2 nanocomposites.

CV curves of the PPy/MoS_2 nanocomposite with various MoS_2 content (wt%) are given in Fig. 7. As the MoS_2 content increases to 33.3 wt%, a maximum CV curve area of PPy/MoS_2 nanocomposite electrode is obtained. However, it is found that the CV curve area of

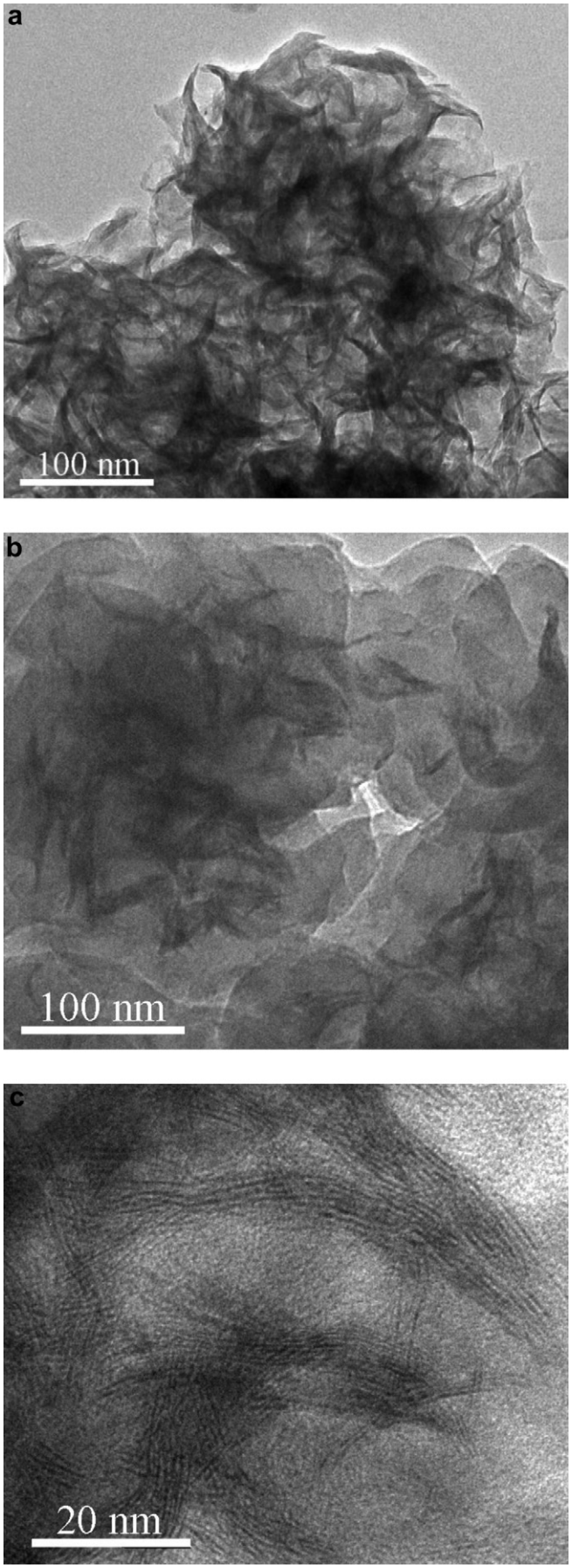

Fig. 4. TEM images of (a) MoS_2 and (b and c) PPy/MoS_2 nanocomposites.

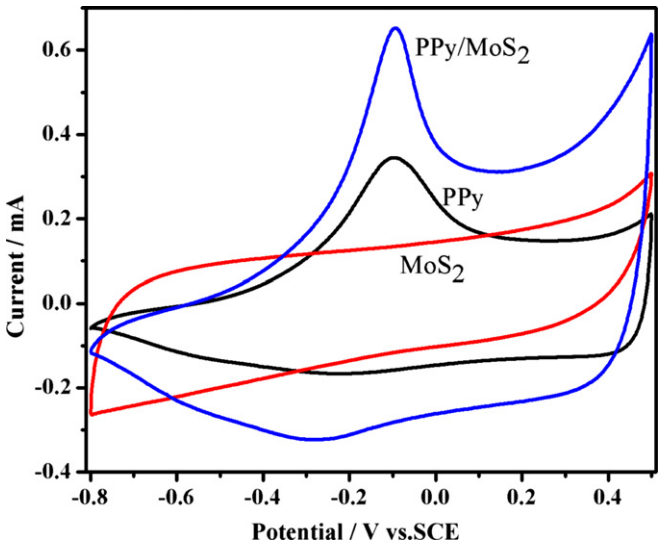

Fig. 5. CV curves of MoS_2, pure PPy and PPy/MoS_2 electrodes at a scan rate 50 mV s^{-1} in 1 M KCl.

PPy/MoS_2 nanocomposite electrode decreases when the MoS_2 content continues to increase to 37.5 wt% or more than it. The PPy are embedded in MoS_2 nanosheets form PPy/MoS_2 nanocomposite, and the sphere-like PPy/MoS_2 nanocomposite with a rough surface would prove more paths for ion diffusion due to their increased interface areas between the electrode material and electrolyte. Therefore, the presence amount of MoS_2 not only as a polymerization substrates in the polymerization system can modify the morphology of PPy, but also provides a path for the insertion and extraction of ions within the PPy, and ensures a high reaction rate. Furthermore, the synergistic effects of the complementary properties of both components, which can be enhance the specific capacitance of PPy/MoS_2 nanocomposite. However, the decrease in the CV curve area is because the capacitance of MoS_2 own limited, a large amount of MoS_2 also does not provide more capacitance.

The galvanostatic charge/discharge is a reliable method to evaluate the electrochemical capacitance of materials. Fig. 8 gives the galvanostatic charge/discharge curves of MoS_2, pure PPy and PPy/MoS_2 composite electrode examined in 1 M KCl electrolyte at a current density of 1 A g^{-1}. The specific capacitance of the electrode can be calculated using the following equation:

$$C_m = C/m = (It)/(\Delta Vm) \quad (3)$$

where C_m is specific capacitance (F g^{-1}), I is charge/discharge current (A), t is the time of discharge (S), ΔV is the voltage difference between the upper and lower potential limits, and m is the mass of the active electrode material. According to the above equation, the specific capacitances of MoS_2, pure PPy and PPy/MoS_2 nanocomposite are 235, 285 and 553.7 F g^{-1} at 1 A g^{-1}, respectively, which is in agreement with the result of the CV curves.

The Fig. 9a presents the charge/discharge curves of the PPy/MoS_2 nanocomposite at various current densities of 1, 2, 3, 5 and 10 A g^{-1}. The discharge capacitances at various current densities are plotted in Fig. 9b. Significantly, the specific capacitance of PPy/MoS_2 nanocomposites still remained as high as 450 F g^{-1} even at a high discharge current density of 10 A g^{-1}. It is evident that the capacitance of this composite slowly decreases as the current density becomes larger. The result indicates the high capacitance of PPy/MoS_2 nanocomposite can be maintained under high current density.

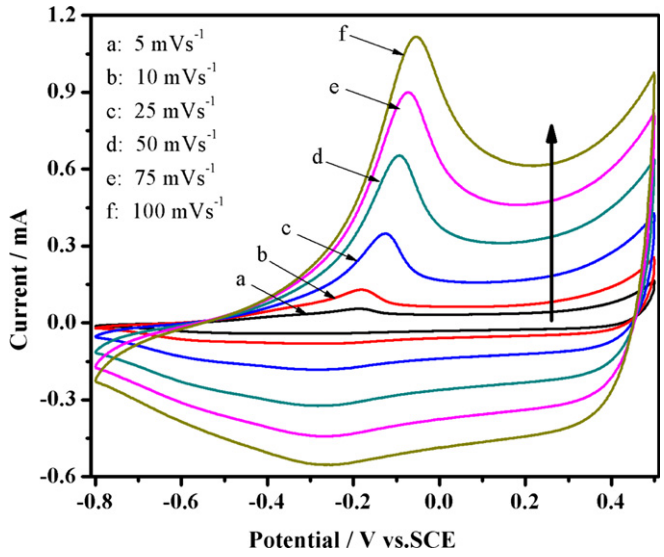

Fig. 6. CV curves of a PPy/MoS_2 electrode at various scan rates in 1 M KCl.

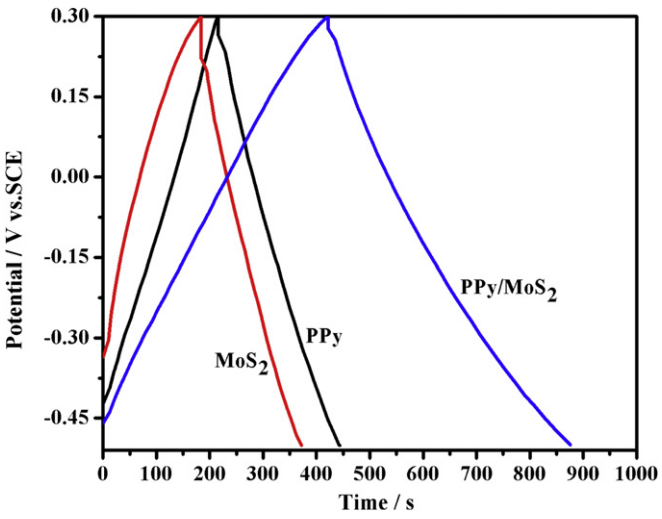

Fig. 8. Galvanostatic charge/discharge curves of MoS_2, pure PPy and PPy/MoS_2 electrodes at a current density of 1 A g^{-1} in 1 M KCl.

The Ragone plots for the MoS_2, pure PPy and PPy/MoS_2 composites are shown in Fig. 10. The energy and power densities were derived from galvanostatic charge/discharge at various current densities. The specific energy density (E) and power density (P) are evaluated according to equations [31]:

$$E = (1/2)CV^2 \quad (4)$$

$$P = E/\Delta t \quad (5)$$

where C is the capacitance of the two-electrode capacitor, V is the voltage decrease in discharge, E is the energy and Δt is the time spent in discharge. As seen from the Ragone plots, as the power density increases from 400 W kg^{-1} to 5700 W kg^{-1}, the energy density of MoS_2, pure PPy decreases from 20.9 Wh kg^{-1} to 8.9 Wh kg^{-1} and decreases from 25.3 Wh kg^{-1} to 9.5 Wh kg^{-1}, respectively. Comparatively, the energy density of the PPy/MoS_2 composite can reach 49.2 Wh kg^{-1} at a power density of 400 W kg^{-1}, and still

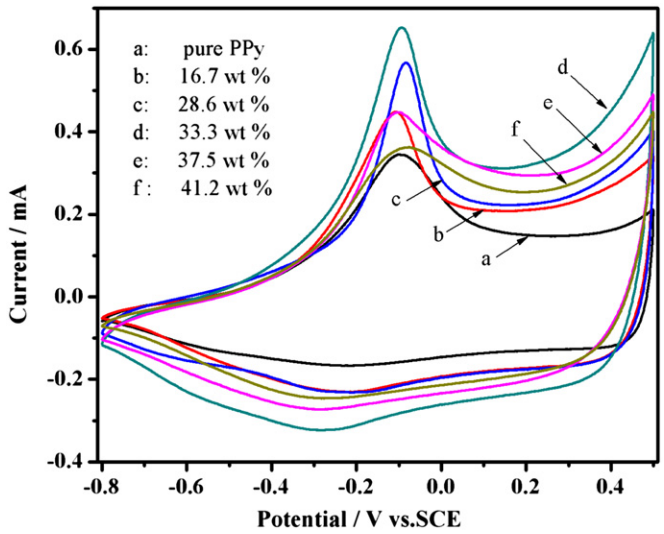

Fig. 7. CV curves of a PPy/MoS_2 electrode with different MoS_2 content (wt%) at scan rate 50 mV s^{-1} in 1 M KCl.

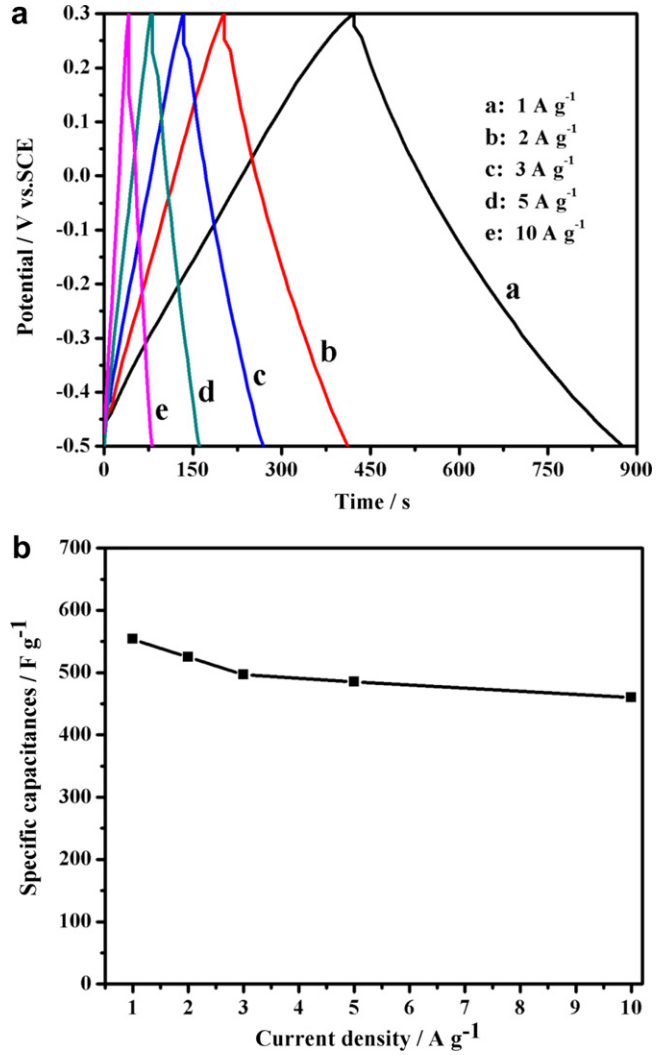

Fig. 9. (a) Galvanostatic charge/discharge curves of PPy/MoS_2 electrodes at various current densities; (b) discharge capacitances at various current densities in 1 M KCl.

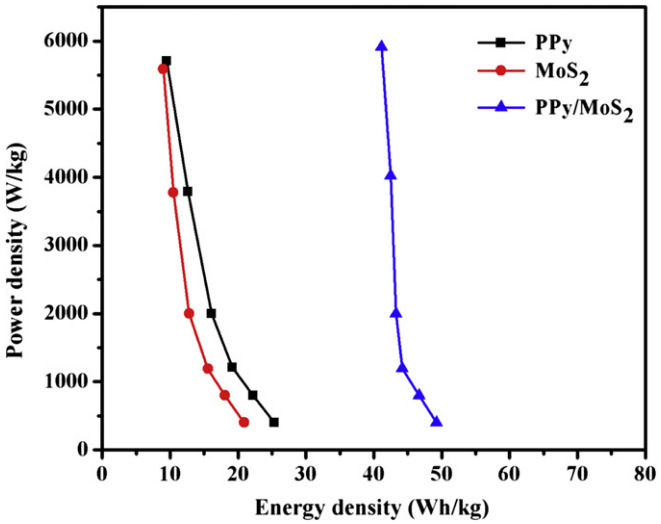

Fig. 10. Ragone plots (power density vs energy density) of MoS_2, pure PPy and PPy/MoS_2 nanocomposites.

remains 41.1 Wh kg^{-1} at a power density of 5800 W kg^{-1}, which exhibited a large power range that can be obtained while maintaining a relatively high energy density. The results illustrate that the PPy/MoS_2 composite materials have excellent electrochemical properties of high energy density and power output.

The cycling stability of MoS_2, pure PPy and PPy/MoS_2 nanocomposite electrodes was measured by charge/discharge cycling at a current density of 1 A g^{-1}, as shown in Fig. 11. The specific capacitance of pure PPy remains only 68.9% after 500 charge/discharge cycles, respectively. However, the PPy/MoS_2 electrode shows a slight decrease and its capacitance still remains about 90% after 500 cycles. PPy has been found to have poor cycling performance mainly due to large volume change during repeated redox cycles which might lead to fatal degradation [31]. However, the thickness of PPy layer on the MoS_2 surface is relatively narrow by this unique hierarchical structure of MoS_2, and the void space between these sheet-like subunits can buffer the volume change during the charge/discharge processes, which has led to enhanced stability of PPy/MoS_2 nanocomposite.

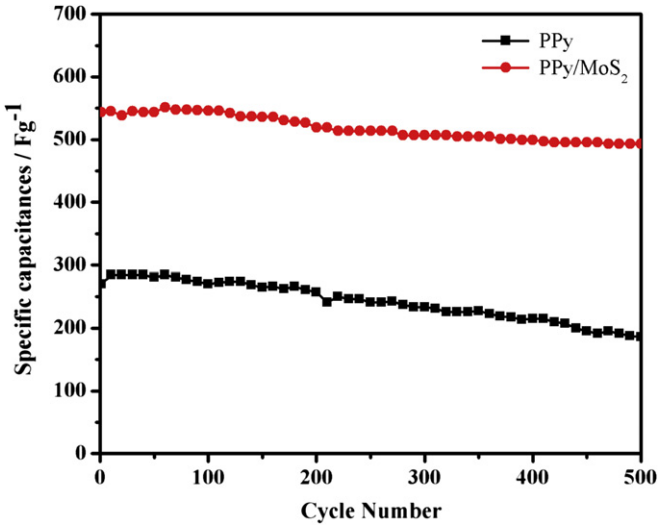

Fig. 11. Variations of the specific capacitances of pure PPy and PPy/MoS_2 electrodes as a function of cycle number measured at the charge/discharge current density of 1 A g^{-1}.

4. Conclusions

It can be concluded that a PPy/MoS_2 nanocomposite with high specific capacitance and long redox cycle life can be obtained by in situ oxidation polymerization of pyrrole in the presence of flowerlike MoS_2 with graphene-like subunits structure suspension. The MoS_2 as polymerization substrates in the polymerization system, thus PPy are embedded in MoS_2 nanosheets form PPy/MoS_2 nanocomposite. The excellent electrochemical properties of PPy/MoS_2 nanocomposite are attributed to the robust composite structure and synergistic effect between PPy and MoS_2. This novel nanocomposite has significant potential to be further exploited in supercapacitor devides.

Acknowledgements

The research was financially supported by the National Science Foundation of China (NO. 21164009, 21174114), the programme for Changjiang Scholars and Innovative Research Team in University (IRT1177), Key Laboratory of Eco-Environment-Related Polymer Materials (Northwest Normal University) of Ministry of Education, and Key Laboratory of Polymer Materials of Gansu Province.

References

[1] P. Simon, Y. Gogotsi, Nat. Mater. 7 (2008) 845–854.
[2] M.D. Stoller, S. Park, Y. Zhu, J. An, R.S. Ruoff, Nano Lett. 8 (2008) 3498–3502.
[3] L.L. Zhang, X.S. Zhao, Chem. Soc. Rev. 38 (2009) 2520–2531.
[4] X.Y. Lang, A. Hirata, T. Fujita, M.W. Chen, Nat. Nanotechnol 6 (2011) 232–236.
[5] Y.W. Zhu, S. Murali, M.D. Stoller, K.J. Ganesh, W.W. Cai, P.J. Ferreira, A. Pirkle, R.M. Wallace, K.A. Cychosz, M. Thommes, D. Su, E.A. Stach, R.S. Ruoff, Science 332 (2011) 1537–1541.
[6] X.H. Lu, D.Z. Zheng, T. Zhai, Z.Q. Liu, Y.Y. Huang, S.L. Xie, Y.X. Tong, Energ. Environ. Sci. 4 (2011) 2915–2921.
[7] G.A. Snooka, P. Kaob, A.S. Bestb, J. Power Sources 196 (2011) 1–12.
[8] F. Schedin, A.K. Geim, S.V. Morozov, E.W. Hill, P. Blake, M.I. Katsnelson, K.S. Novoselov, Nat. Mater. 6 (2007) 652–655.
[9] W. Shi, J. Zhu, D.H. Sim, Y.Y. Tay, Z.Y. Lu, X.J. Zhang, H. Zhang, H.H. Hng, Q. Yan, J. Mater. Chem. 21 (2011) 3422–3427.
[10] A. Reina, X.T. Jia, J. Ho, D. Nezich, H.B. Son, V. Bulovic, M.S. Dresselhaus, J. Kong, Nano Lett. 9 (2009) 30–35.
[11] D.V. Kosynkin, A.L. Higginbotham, A. Sinitskii, J.R. Lomeda, A. Dimiev, B.K. Price, J.M. Tour, Nature 458 (2009) 872–876.
[12] H.S.S. Ramakrishna Matte, A. Gomathi, A.K. Manna, D.J. Late, R. Datta, S.K. Pati, C.N.R. Rao, Angew. Chem. Int. Ed. 122 (2010) 4153–4162.
[13] R. Tenne, L. Margulis, M. Genut, G. Hodes, Nature 360 (1992) 444–446.
[14] A.V. Powell, L. Kosidowski, A. McDowall, J. Mater. Chem. 11 (2001) 1086–1091.
[15] J. Xiao, D.W. Choi, L. Cosimbescu, P. Koech, J. Liu, J.P. Lemmon, Chem. Mater. 22 (2010) 4522–4524.
[16] D. Merki, X.L. Hu, Energ. Environ. Sci. 4 (2011) 3878–3888.
[17] K. Chang, W.X. Chen, Chem. Commun. 47 (2011) 4252–4254.
[18] Y.G. Li, H.L. Wang, L.L. Xie, Y.Y. Liang, G.S. Hong, H.J. Dai, J. Am. Chem. Soc. 133 (2011) 7296–7299.
[19] Z. Yin, H. Li, H. Li, L. Jiang, Y. Shi, Y. Sun, G. Lu, Q. Zhang, X. Chen, H. Zhang, ACS Nano 6 (2012) 74–80.
[20] J.M. Soon, K.P. Loh, Electrochem. Solid-state Lett. 10 (2007) A250–A254.
[21] S. Ghosh, O. Inganäs, Adv. Mater. 11 (1999) 1214–1218.
[22] L. Fan, J. Maier, Electrochem. Commun. 8 (2006) 937–940.
[23] H.F. An, Y. Wang, X.Y. Wang, L.P. Zheng, X.Y. Wang, L.H. Yi, L. Bai, X.Y. Zhang, J. Power Sources 195 (2010) 6964–6969.
[24] Y. Yan, Q. Cheng, G. Wang, C. Li, J. Power Sources 196 (2011) 7835–7840.
[25] X.J. Lu, H. Dou, C.Z. Yuan, S.D. Yang, L. Hao, F. Zhang, L.F. Shen, L.J. Zhang, X.G. Zhang, J. Power Sources 197 (2012) 319–324.
[26] R.K. Sharma, A.C. Rastogi, S.B. Desu, Electrochim. Acta 53 (2008) 7690–7695.
[27] H. Peng, G.F. Ma, W.M. Ying, A.D. Wang, H.H. Huang, Z.Q. Lei, J. Power Sources 211 (2012) 40–45.
[28] X. Wang, H. Bai, G. Shi, J. Am. Chem. Soc. 133 (2011) 6338–6342.
[29] X.L. Li, Y.D. Li, J. Phys. Chem. B 37 (2004) 13893–13900.
[30] C.Z. Zhu, J.F. Zhai, D. Wen, S.J. Dong, J. Mater. Chem. 22 (2012) 6300–6306.
[31] R. Kötz, M. Carlen, Electrochim. Acta 45 (2000) 2483–2498.